Human Molecular Genetics, 2010, Vol. 19, No. 6 **1033–1047**
doi:10.1093/hmg/ddp567
Advance Access published on December 22, 2009

Disease mutations in Rab7 result in unregulated nucleotide exchange and inappropriate activation

Brett A. McCray[1,2], Emmanuel Skordalakes[3] and J. Paul Taylor[1,*]

[1]Department of Developmental Neurobiology, St Jude Children's Research Hospital, Memphis, TN 38105, USA, [2]Neuroscience Graduate Group, University of Pennsylvania School of Medicine, Philadelphia, PA 19104, USA and [3]Gene Expression and Regulation Program, The Wistar Institute, Philadelphia, PA 19104, USA

Received October 7, 2009; Revised November 23, 2009; Accepted December 21, 2009

Rab GTPases are molecular switches that orchestrate vesicular trafficking, maturation and fusion by cycling between an active, GTP-bound form, and an inactive, GDP-bound form. The activity cycle is coupled to GTP hydrolysis and is tightly controlled by regulatory proteins. Missense mutations of the GTPase Rab7 cause a dominantly inherited axonal degeneration known as Charcot-Marie-Tooth type 2B through an unknown mechanism. We present the 2.8 Å crystal structure of GTP-bound L129F mutant Rab7 which reveals normal conformations of the effector binding regions and catalytic site, but an alteration to the nucleotide binding pocket that is predicted to alter GTP binding. Through extensive biochemical analysis, we demonstrate that disease-associated mutations in Rab7 do not lead to an intrinsic GTPase defect, but permit unregulated nucleotide exchange leading to both excessive activation and hydrolysis-independent inactivation. Consistent with augmented activity, mutant Rab7 shows significantly enhanced interaction with a subset of effector proteins. In addition, dynamic imaging demonstrates that mutant Rab7 is abnormally retained on target membranes. However, we show that the increased activation of mutant Rab7 is counterbalanced by unregulated, GTP hydrolysis-independent membrane cycling. Notably, disease mutations are able to rescue the membrane cycling of a GTPase-deficient mutant. Thus, we demonstrate that disease mutations uncouple Rab7 from the spatial and temporal control normally imposed by regulatory proteins and cause disease not by a gain of novel toxic function, but by misregulation of native Rab7 activity.

INTRODUCTION

Members of the Rab family of small GTPases such as Rab7 are master regulators of vesicular trafficking, maturation and fusion. Rab GTPases function as molecular switches by cycling between active, GTP-bound states in which they are reversibly associated with specific vesicular membranes and inactive, GDP-bound states in which they are predominantly cytosolic and dissociated from their target membranes. Following GTP binding, Rabs recruit specific effector proteins that are involved in vesicular transport and hetero- and homotypic fusion events. For each of the more than 60 human Rabs, multiple regulatory proteins have evolved to modulate Rab membrane targeting and activity. Inactive Rabs are largely sequestered in the cytosol by Rab GDP-dissociation inhibitor (GDI) which recognizes GDP-bound Rabs and binds their C-terminal geranylgeranyl group (1,2). Activation of Rabs requires extraction from Rab GDI, insertion into membranes and GTP exchange. To facilitate GTP exchange, guanine nucleotide exchange factors (GEFs) bind the GDP-bound conformation of Rabs and lead to structural alterations that facilitate GDP release and allow subsequent GTP binding (3). Two 'switch' regions of Rabs undergo conformational changes depending on the identity of the bound guanine nucleotide. Rab effector proteins specifically recognize the GTP-bound conformation of the switch regions and are therefore recruited only to activate Rabs. Termination of Rab function is mediated through hydrolysis of the γ-phosphate of GTP to yield GDP. GTPase activating proteins (GAPs) accelerate the hydrolysis reaction by catalyzing the nucleophilic attack

*To whom correspondence should be addressed at: Department of Developmental Neurobiology, St Jude Children's Research Hospital, 262 Danny Thomas Place, MS 343, D-4026, Memphis, TN 38105-3678, USA. Tel: +1 9015956047; Fax: +1 9015952032; Email: jpaul.taylor@stjude.org

of a water molecule on the γ-phosphate of GTP. Following hydrolysis, GDP-bound Rabs are recognized and extracted from the membrane by GDI (4). Thus, GEF and GAP proteins along with GDI play a critical role in the regulation of the Rab activity cycle.

Rab7 is a ubiquitously expressed protein that plays a vital role in the regulation of the trafficking, maturation and fusion of endocytic and autophagic vesicles. Rab7 localizes primarily to acidic, pre-degradative and degradative organelles such as late endosomes, lysosomes, multivesicular bodies, phagosomes, autophagosomes and autophagolysosomes (5–8). Rab7 specifically controls the transition of early endosomes into the late-endosomal/lysosomal system and subsequent degradation of cargos associated with target vesicles. As such, Rab7 activity regulates the lysosome-mediated degradation of endocytic cargos such as activated EGF receptors, internalized cholesterol and neurotrophic factor receptors such as TrkA (6,9,10). In addition, fusion of autophagic vacuoles with lysosomes requires Rab7 activity (11,12). Rab7 has also been implicated in the regulation of long-range axonal trafficking (13). Although there is no consensus as to the exact role of Rab7 in axonal transport, evidence suggests that Rab5 and Rab7 together regulate the retrograde trafficking of signaling endosomes that supply trophic support to neurons in the peripheral nervous system (14).

Charcot-Marie-Tooth disease comprises a heterogeneous group of inherited peripheral neuropathies (15). Patients with CMT present with length-dependent sensory, motor or autonomic dysfunction either alone or in combination. Two major subtypes of CMT are recognized and distinguished by the primary pathology. CMT type 1 is characterized by prominent demyelination and decreased nerve conduction velocities and is most commonly caused by mutations in myelin-specific proteins. In contrast, the primary pathological feature in CMT type 2 is axonal degeneration. Although genetic mutations that cause CMT type 2 affect a variety of cellular processes, defects in mitochondrial physiology, chaperone activity and axonal transport pathways are most commonly implicated (16). To date, four missense mutations in Rab7 have been associated with Charcot-Marie-Tooth disease type 2B (OMIM 600882) (17–19). This subtype of CMT is distinguished by profound loss of pain sensation leading to recurrent ulcers, deformities and frequent need for amputation of the lower limbs (20). As such, CMT2B is alternatively classified as ulcero-mutilating neuropathy. Degeneration of motor neurons and subsequent muscle weakness are also associated with CMT2B (20).

At present, it is unknown how mutations in Rab7 lead to axonal degeneration. A prior study suggested that disease mutations reduce nucleotide affinity, impair Rab7 GTPase activity and lead to constitutive activation (21). However, the finding of decreased hydrolysis in disease mutants was enigmatic given that the mutations are not localized near the catalytic site. Therefore, we set out to precisely define the impact of disease-causing mutations on Rab7 structure and function in order to illuminate the mechanism of pathogenesis. We determined the crystal structure of GTP-bound L129F mutant Rab7 at 2.8 Å resolution revealing an alteration to the nucleotide binding pocket, but no impact on the catalytic region of Rab7. These findings guided biochemical analyses in which we determined that disease-causing mutations in Rab7 do not lead to an intrinsic GTPase defect, but instead result in decreased nucleotide affinity and permit unregulated nucleotide exchange. We report that misregulation of Rab7 activation results in an increase in the active fraction of Rab7 and abnormal retention on target membranes. However, we also show that the excessive activation of Rab7 mutants is counterbalanced by unregulated, GTP hydrolysis-independent cycling, thus ruling out constitutive activation of mutant Rab7 as a pathogenic mechanism for CMT2B. We also used an unbiased approach to interrogate the protein interactors of wild-type and mutant forms of Rab7. As predicted by our structural data, the complement of interactors in wild-type and mutant Rab7 is qualitatively identical, although there is significantly enhanced interaction of mutant Rab7 with a subset of effector proteins. This study reveals a pathogenic mechanism wherein disease mutations uncouple Rab7 from normal spatial and temporal regulatory restraints resulting in toxic misregulation of Rab7 activity.

RESULTS

The L129F mutation alters the nucleotide binding pocket of Rab7

Rab GTPases cycle between activate, GTP-bound, membrane-associated states and inactive, GDP-bound, cytosolic states. Mutations in Rab7 that cause CMT2B cluster near the highly conserved G-loops that are involved in nucleotide binding. A previous study demonstrated decreased GTP hydrolysis in disease mutants (21). However, as residues mutated in CMT2B are not near the catalytic glutamine (Q67) or the hydrolyzed γ-phosphate of GTP, it was unclear how disease mutations could impair GTPase activity. To resolve this issue and provide mechanistic insight into CMT2B, we solved the crystal structure of the L129F Rab7 mutant in its active, GTP-bound form. The structure of full-length L129F Rab7 bound to the non-hydrolysable GTP analog GppNHp was solved to 2.8 Å by molecular replacement (MR) using wild-type Rab7 as a search model (Table 1). The L129F substitution does not alter the overall structure of the molecule as compared to the published structure of wild-type Rab7 bound to GppNHp (PDB 1VG8) (Fig. 1A–C, Supplementary Material, Fig. S1 for stereo views) (22). Notably, the conformation of the effector binding switch region of the protein closely approximates that of wild-type Rab7 and is therefore not predicted to alter effector binding. Furthermore, the catalytic glutamine (Q67) and the position of the γ-phosphate group of GppNHp were not significantly altered, providing no structural basis to predict decreased intrinsic GTPase activity (Fig. 1D, Supplementary Material, Fig. S2 for an omit map of the nucleotide binding pocket). However, L129F substitution enlarges the hydrophobic group that lies adjacent to the guanine ring of GTP and leads to steric hindrance and subtle repositioning (∼0.6 Å) of the guanine ring away from F129 (Fig. 1D–F, Supplementary Material, Fig. S3 for stereo views). This also slightly modifies the position of the invariant D128 and

Table 1. Data collection and refinement statistics

Data collection	
Space group	*P*1
Cell dimensions (*a*, *b*, *c* in Å)	35.6, 89.33, 89.38
Resolution (Å)	20–2.8 (2.9–2.8)[a]
R_{sym} or R_{merge}	10.0 (41.7)
$I/\sigma I$	7.7 (1.7)
Completeness (%)	98.7 (98.2)
Redundancy	2 (2)
Refinement	
Resolution (Å)	20–2.8
No. unique reflections	27713
R_{work}/R_{free}	25.5/27.1
No. atoms	
Protein	6925
Ligands	155
Ions	5
Water	45
R.m.s. deviations	
Bond lengths (Å)	0.011
Bond angles (°)	1.16
Ramachandran plot (%)	
Most favored	87.6
Allowed	10.9
Generously allowed	1.2
Disallowed	0.2

[a]Highest resolution shell shown in parentheses.

K157 residues that are directly involved in nucleotide binding (Fig. 1D). Of particular note is the repositioning of the carboxylate group of D128, which in the wild-type Rab7 makes pseudo Watson–Crick pairing interactions with the guanine base of the nucleotide. In L129F, this interaction appears to be partially altered leading to longer hydrogen bonds and in some cases (we have five molecules in the asymmetric unit and therefore five independent observations) complete disruption of one of the two hydrogen bonds. We predicted that these changes would alter affinity for guanine nucleotides and affect the rates of dissociation for GTP and/or GDP. Interestingly, K157, which is also directly involved in nucleotide binding and is shifted in the L129F mutant structure, is mutated to asparagine in a patient with CMT2B (19).

Mutant Rab7 has decreased nucleotide affinity, but no intrinsic GTPase defect

To determine how the steric hindrance imposed by the L129F mutation affects guanine nucleotide binding, we performed GTP and GDP dissociation assays using purified recombinant wild-type and L129F Rab7. We also analyzed the V162M mutant to determine whether there are consistent biochemical alterations among different disease-causing Rab7 mutants. Recombinant Rab7 proteins were loaded with ^{3}H-GTP or ^{3}H-GDP and the dissociation of nucleotide was followed over time. We found that Rab7 mutants have an increased rate of GTP dissociation relative to wild-type (Fig. 2A), and an even more rapid rate of GDP dissociation with almost complete dissociation within 15 min (Fig. 2B). These results are consistent with the previous work showing increased dissociation of guanine nucleotides in Rab7 disease mutants (21). In Rab7 mutants, ~70% of initially bound GTP dissociated over the course of 60 min.

Although Rab7 disease mutants were previously reported to have nearly complete loss of GTPase activity (21), we found no structural basis for altered GTP hydrolysis in the L129F mutant. To account for this discrepancy, we hypothesized that reduced hydrolysis might reflect increased rates of GTP dissociation rather than an intrinsic catalytic defect. To test this idea, we first performed GTPase assays using purified recombinant Rab7 as previously described (21). When Rab7 was loaded with ^{32}P-GTP and hydrolysis was initiated in the presence of excess unlabeled GTP, we saw a marked decrease in GTP hydrolysis in the L129F mutant that was similar to the Q67L mutant which contains a targeted disruption of the catalytic residue (Fig. 2C and D, left). However, this assay specifically measures the rate of GTP hydrolysis *per GTP binding event*, because re-association of ^{32}P-GTP is effectively precluded by the excess unlabeled GTP. We predicted that if we performed the assay with excess ^{32}P-GTP and no unlabeled GTP, we could counteract the effect of decreased nucleotide affinity by allowing for dissociation and re-association of radiolabeled GTP. Indeed, we found that the apparent GTPase defect in the L129F mutant could be partially rescued by omitting excess unlabeled GTP from the reaction, whereas this modification had no effect on the Q67L mutant (Fig. 2C, right and D). Furthermore, increasing the concentration of ^{32}P-GTP further restored catalytic activity (Fig. 2E), indicating that dissociation and re-association of GTP happens rapidly in disease mutants and that catalytic activity of L129F Rab7 approaches that of wild-type Rab7. Thus, when GTP is in constant supply (as is the case *in vivo*), catalytic activity in disease mutants is not significantly impaired, and decreased GTP hydrolysis cannot account for the defects seen in mutant Rab7.

Mutant Rab7 undergoes GEF-independent nucleotide exchange and excessive activation

Normally, GDP is tightly bound by Rab GTPases, and the low intrinsic rate of GDP dissociation makes GDP release the rate-limiting step of nucleotide exchange and Rab activation. GEF proteins have evolved to facilitate GDP dissociation and the subsequent GTP loading of Rab proteins. Given the rapid rate of GDP dissociation in the Rab7 disease mutants, we hypothesized that nucleotide exchange might be misregulated and occur independent of GEF activity. To test this hypothesis, we interrogated GTP exchange rates using purified, recombinant Rab7 proteins in the absence of any GEF activity. First, we determined that Rab7 wild-type and disease mutants bound roughly the same amount of GTP following stripping of endogenous bound nucleotide (Fig. 3A). Next, we tested GTP exchange by stripping endogenous nucleotide, then pre-loading the Rab7 proteins with GDP before incubation with ^{3}H-GTP. In this assay, ^{3}H-GTP binding requires dissociation of the pre-loaded GDP and thus represents the rate of GTP exchange. The amount of ^{3}H-GTP bound was compared with the maximum amount that could be bound without GDP pre-incubation. As expected, wild-type Rab7 showed a slow rate of GTP exchange in the absence of GEF activity (only 10–20% of maximal binding). However, disease-causing

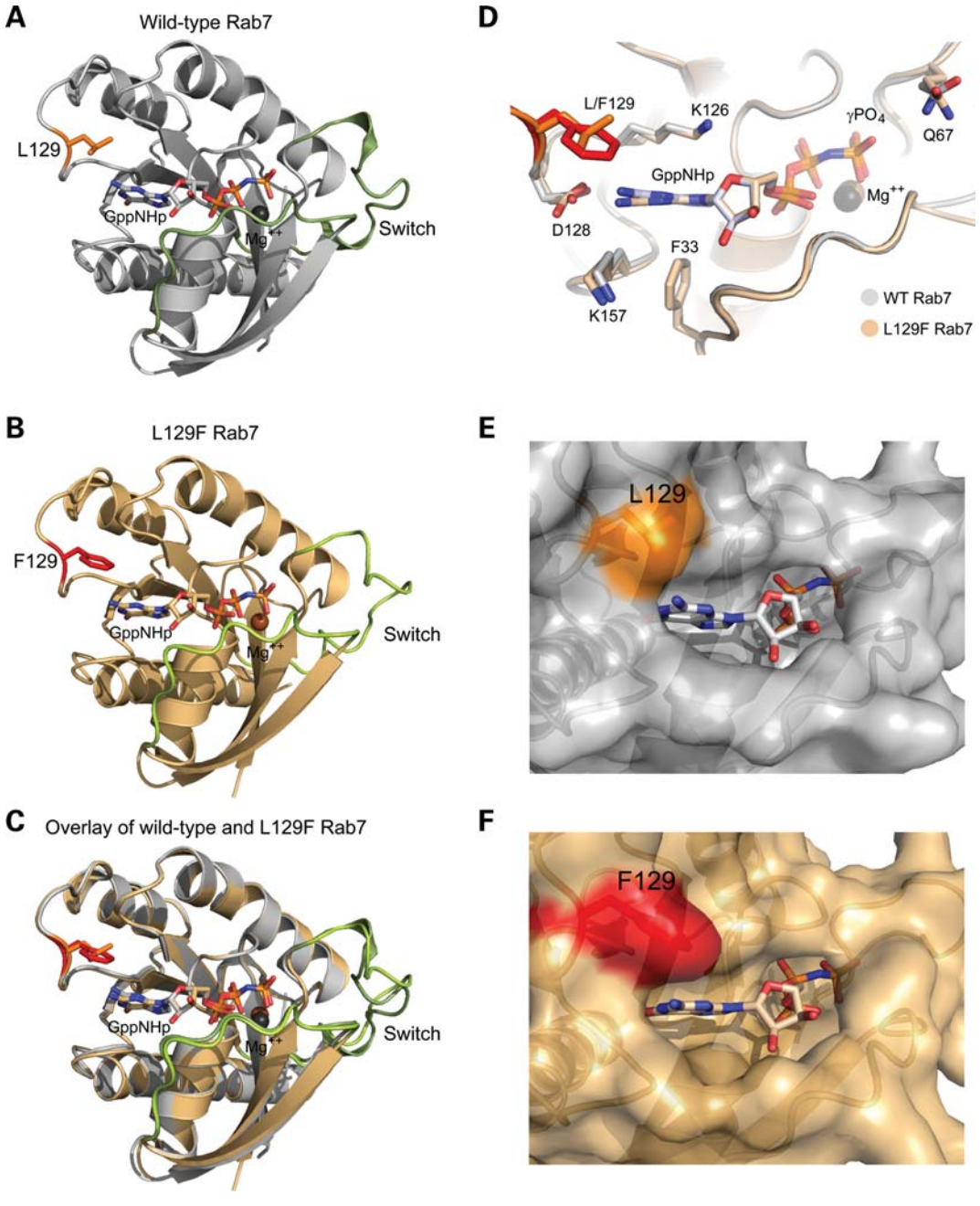

Figure 1. Structural insights into the disease-causing Rab7 L129F mutant. (**A**) Structure of wild-type Rab7 bound to the non-hydrolysable GTP analog GppNHp (PDB 1VG8) (24). Switch regions are shown in dark green, L129 in orange and Mg^{++} in black. (**B**) Structure of Rab7 L129F. Switch regions are shown in light green, F129 in red and Mg^{++} in dark brown. (**C**) Overlay of wild-type and L129F Rab7 demonstrates that the F129 mutation does not alter the overall structure of the protein. Note the normal conformation of the switch regions in the L129F mutant. (**D**) Close-up, overlaid views of the binding pockets of wild-type (gray) and the F129 mutant (brown). The positions of the γ-phosphate group of GTP and the catalytic residue Q67 are unaltered by the F129 mutation. Note the shift of the guanine ring of GppNHp in F129 and the displacement of the K157 and D128 residues. These changes suggest alterations in nucleotide binding affinity. (**E**) Detailed surface representation of the wild-type guanine nucleotide binding pocket showing GppNHp in stick representation and L129 in orange. (**F**) Detailed surface representation of the F129 guanine nucleotide binding pocket showing GppNHp in stick representation and F129 in red. Note the slight change in position of the guanine ring of the nucleotide and the altered conformation of the opening to the binding pocket.

Rab7 mutants underwent GTP exchange significantly faster, achieving nearly 60% of maximal binding over 30 min (Fig. 3B). This suggests that GTP exchange in Rab7 mutants can occur in an unregulated, GEF-independent manner. To determine whether GTP exchange is also misregulated in a cellular context, we tested the ability of immunopurified Rab7 complexes to undergo guanine nucleotide exchange. FLAG–Rab7 was immunopurified from HEK293T cell lysates and then incubated with ^{3}H-GTP. As in the cell-free system, Rab7 mutants were able to undergo nucleotide

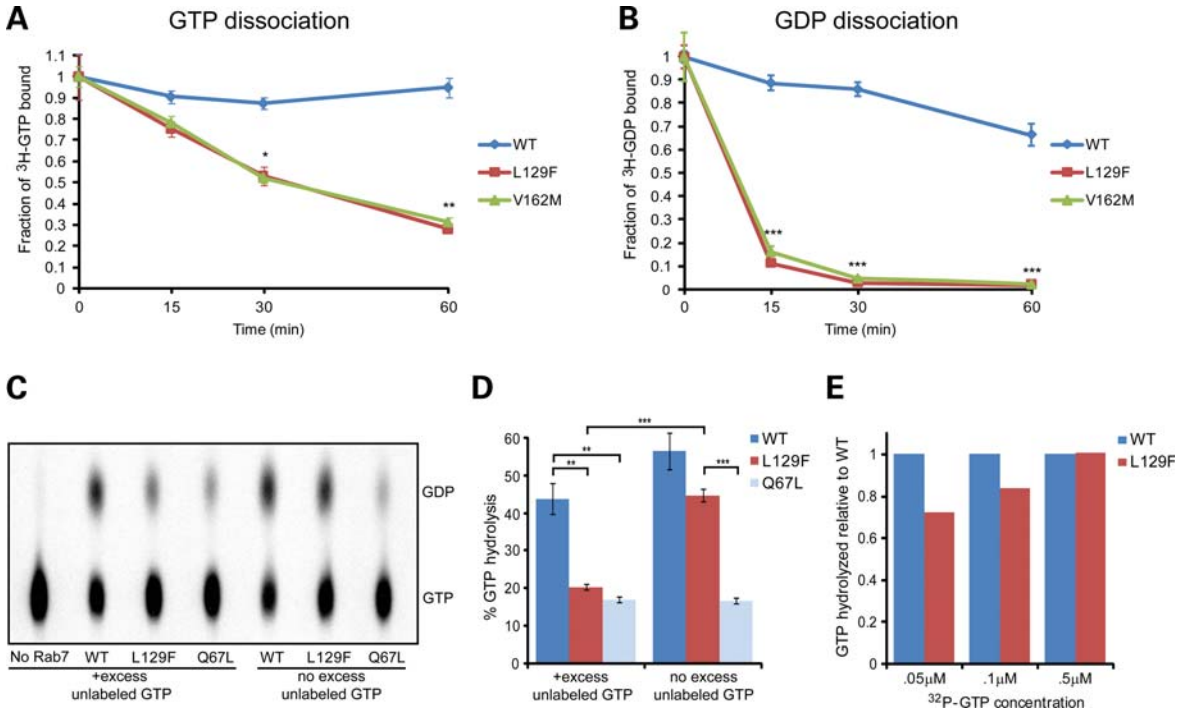

Figure 2. Rab7 disease-causing mutants have increased guanine nucleotide dissociation, but nearly normal GTPase activity. (**A**–**B**) GTP (A) and GDP (B) dissociation rates of recombinant Rab7 proteins. Rab7 mutants were loaded with ^{3}H-GTP or ^{3}H-GDP, then washed and incubated with excess unlabeled GTP or GDP at 37°C for 0, 15, 30 or 60 min. The remaining bound ^{3}H-GTP or ^{3}H-GDP was then eluted and quantified by scintillation counting. (**C**) Representative GTPase assay of wild-type, L129F and Q67L Rab7. His-MBP-Rab7 proteins were loaded with 0.1 μM ^{32}P-GTP on ice, then moved to 37°C for 2 h to allow for hydrolysis. Nucleotides were eluted and separated by thin layer chromatography. GTPase assays performed with excess unlabeled GTP during hydrolysis (left) reveal a marked reduction in hydrolysis in the L129F mutant. However, assays performed without excess unlabeled GTP during hydrolysis (right) demonstrate that catalytic activity in the L129F mutant is restored by a constant supply of ^{32}P-GTP. Hydrolysis is virtually undetectable when no Rab7 is added to the reaction (left). (**D**) Quantification of GTPase assays demonstrates nearly complete restoration of catalytic activity in the L129F mutant when ^{32}P-GTP is provided in constant supply. As expected, the GTPase-deficient Q67L mutant shows a marked hydrolysis defect in both conditions. (**E**) GTPase assays were performed with varying concentrations of ^{32}P-GTP and without excess unlabeled GTP. Increasing the GTP concentration restores the catalytic activity of the L129F mutant. This suggests that there is no intrinsic GTPase defect in disease mutants when GTP is in constant supply. Values plotted for (A–D) represent the average of at least three independent experiments. Error bars represent standard error of the mean ($^{*}P < 0.05$, $^{**}P < 0.01$, $^{***}P < 0.001$).

exchange more readily than wild-type Rab7 despite equal immunoprecipitation of Rab7 in each condition (Fig. 3C). These results indicate that the structural changes imposed by the L129F and V162M mutations lead to misregulation of GTP exchange and inappropriate activation of Rab7 mutants.

Augmented GTP exchange in the disease mutants would be predicted to shift the ratio of the GTP and GDP-bound fractions of Rab7 in cells. To test this, we performed pull-down assays using an immobilized Rab7 binding region of the Rab7 effector Rab-interacting lysosomal protein (RILP) and lysates from HEK293T cells expressing GFP–Rab7 (23). As RILP specifically binds GTP-bound Rab7, the amount of Rab7 associated with RILP in this assay represents the GTP-bound fraction. GST-RILP showed increased interaction with the predominantly GTP-bound, GTPase-deficient Q67L mutant and no interaction with the GTP-binding deficient T22N mutant, indicating that this experiment accurately reflects changes in the active pool of Rab7 (Fig. 3D). The amount of Rab7 disease-causing mutants pulled down by GST-RILP was significantly increased compared with wild-type Rab7 (Fig. 3D and E). This finding indicates that accelerated GTP exchange in disease mutants leads to an increase in the active, GTP-bound fraction of Rab7.

Disease-causing mutations cause quantitative changes in Rab7 interactions

To more broadly address the impact of disease-causing Rab7 mutations on interaction with binding partners, we used an unbiased proteomics approach to examine the protein–protein interactions in wild-type and mutant Rab7. Rab7 effectors specifically recognize the switch regions when Rab GTPases are in the GTP-bound conformation. On the basis of the crystal structure, we predicted that the L129F Rab7 mutant would interact normally with Rab7 effectors. However, as Rab7 mutations increase the fraction of Rab7 in the active conformation and cause misregulation of the Rab7 activity cycle, we predicted that there may be quantitative differences in the type of Rab7 complexes that are formed. A number of Rab7-interacting proteins have been described, including RILP, Oxysterol binding protein-related protein 1L (ORP1L), Rabring7, Rab escort protein-1 (REP-1), Rab GDI, the Vps34 subunit of PI3 kinase and members of the retromer complex (24–30).

To examine Rab7 interactors, FLAG–Rab7 complexes were immunopurified from HEK293T cell lysates, separated by SDS–PAGE and interacting proteins were then identified

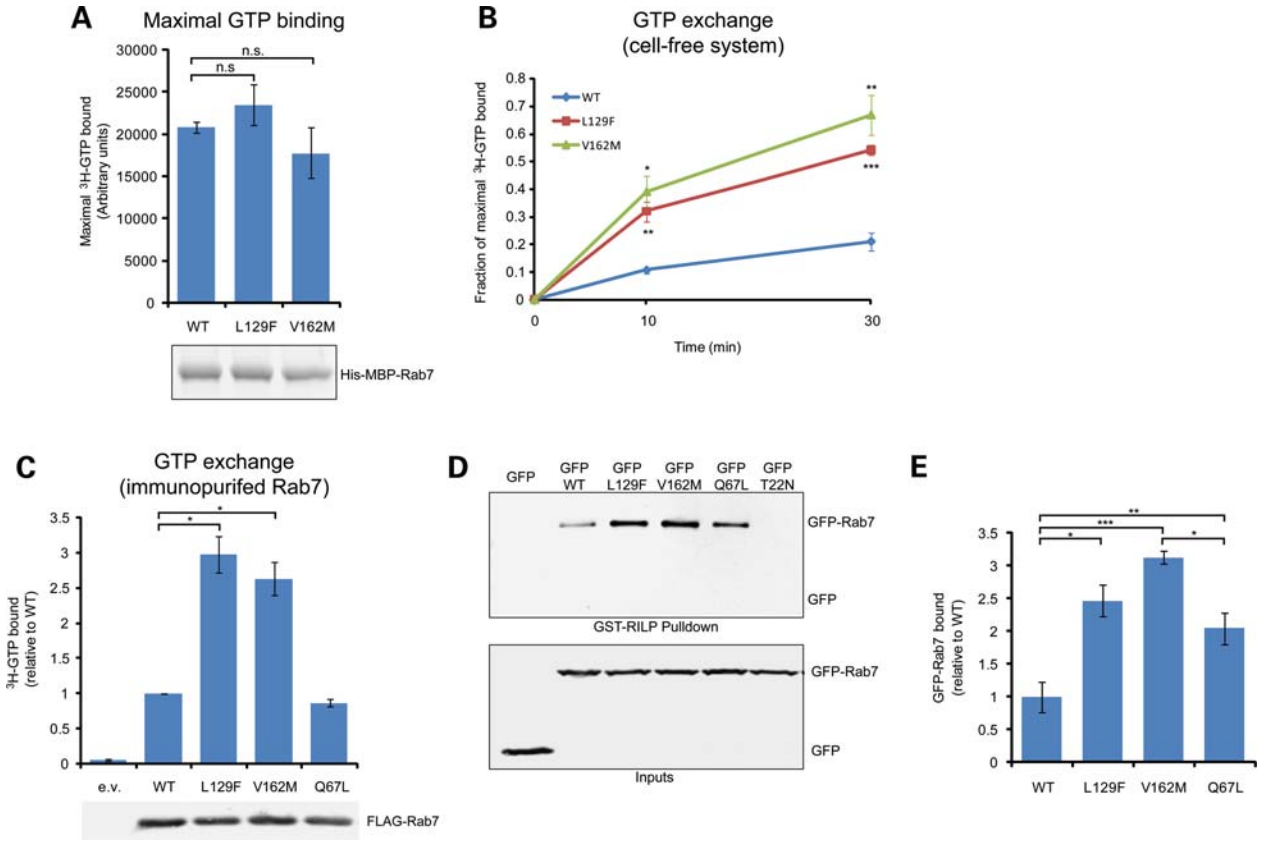

Figure 3. Rab7 disease mutants lead to GEF-independent nucleotide exchange. (**A**) Top: purified His-MBP-Rab7 proteins were stripped of endogenous nucleotide and then incubated with ^{3}H-GTP for 30 min at 37°C to demonstrate equivalent maximal GTP binding. Bottom: loading control shows equivalent amount of Rab7 protein in each condition. (**B**) Quantification of GTP exchange of Rab7 proteins. His-MBP-Rab7 proteins were stripped, loaded with GDP and then incubated with ^{3}H-GTP for 10 or 30 min at 37°C. Disease mutants exchanged GTP for GDP much faster than wild-type Rab7 ($^{*}P < 0.05$, $^{**}P < 0.01$, $^{***}P < 0.005$). (**C**) Top: GTP exchange assay using immunopurified FLAG–Rab7. FLAG–Rab7 proteins were immunopurified from HEK293T cells followed by incubation with ^{3}H-GTP for 10 min at 37°C. Rab7 disease mutants undergo greater nucleotide exchange compared with wild-type ($^{*}P < 0.005$). Bottom: control immunoprecipitation performed in parallel demonstrates equal immunoprecipitation of FLAG–Rab7 constructs. (**D**) Top: representative immunoblot of GST-RILP pull-down from HEK293T lysates containing GFP–Rab7. GST-RILP pulls down more Rab7 disease mutant protein indicating an increase in the GTP-bound form. As expected, there is increased binding of Q67L and no binding of T22N Rab7. Bottom: immunoblot of 2% of the pull-down input demonstrates equivalent expression of GFP–Rab7 in each condition. (**E**) Quantification of GST-RILP pull-down replicates ($^{*}P < 0.02$, $^{**}P < 0.05$, $^{***}P < 0.002$). All values plotted represent the average of three independent experiments. Error bars represent standard error of the mean. e.v. = empty vector.

by mass spectrometry. The profiles of proteins identified in wild-type and mutant Rab7 were qualitatively identical, suggesting that Rab7 mutants bind to the same complement of interactors as wild-type Rab7 (Fig. 4A and B, Supplementary Material, Fig. S4). We identified several putative novel Rab7 interacting proteins as well as previously known Rab7 interactors (Table 2). To verify the specificity of our mass spectrometry protein identification, interactions with the known effectors RILP and GDI2 and the novel interactors VapB, SPG21, PHB and stomatin-like 2 were confirmed by coimmunoprecipitation followed by western blotting (Supplementary Material, Fig. S5).

Although the complement of effectors is largely unchanged by disease-causing mutations, we were able to detect quantitative differences in the amount of specific effectors coimmunoprecipitated with wild-type and mutant Rab7 (Fig. 4B and C). Specifically, Rab7 disease mutants L129F and V162M and the constitutively active mutant Q67L showed increased interaction with Vps13C and ORP1L, whereas only the disease mutants showed increased interaction with clathrin heavy chain, and all constructs interacted equally with REP-1 (Fig. 4C). These results suggest that the misregulation of the Rab7 activity cycle in disease mutants leads to the augmentation of specific effector interactions. Furthermore, the increased interaction with Vps13C and the GTP-dependent interactor ORP1L seen in disease mutants and in the Q67L mutant provides additional support for an increase in the active fraction of mutant Rab7.

Rab7 disease mutant localization is distinct from constitutively active Rab7

We next assessed the consequences of the structural and biochemical alterations in mutant Rab7 on membrane targeting and exchange dynamics. To determine whether disease mutations affect Rab7 subcellular localization, we analyzed the distribution of GFP-tagged Rab7 in HeLa cells. Wild-type Rab7 reversibly associates with the cytosolic face of late endosomes, lysosomes and autophagosomes and shows a diffuse vesicular pattern that largely overlaps with the

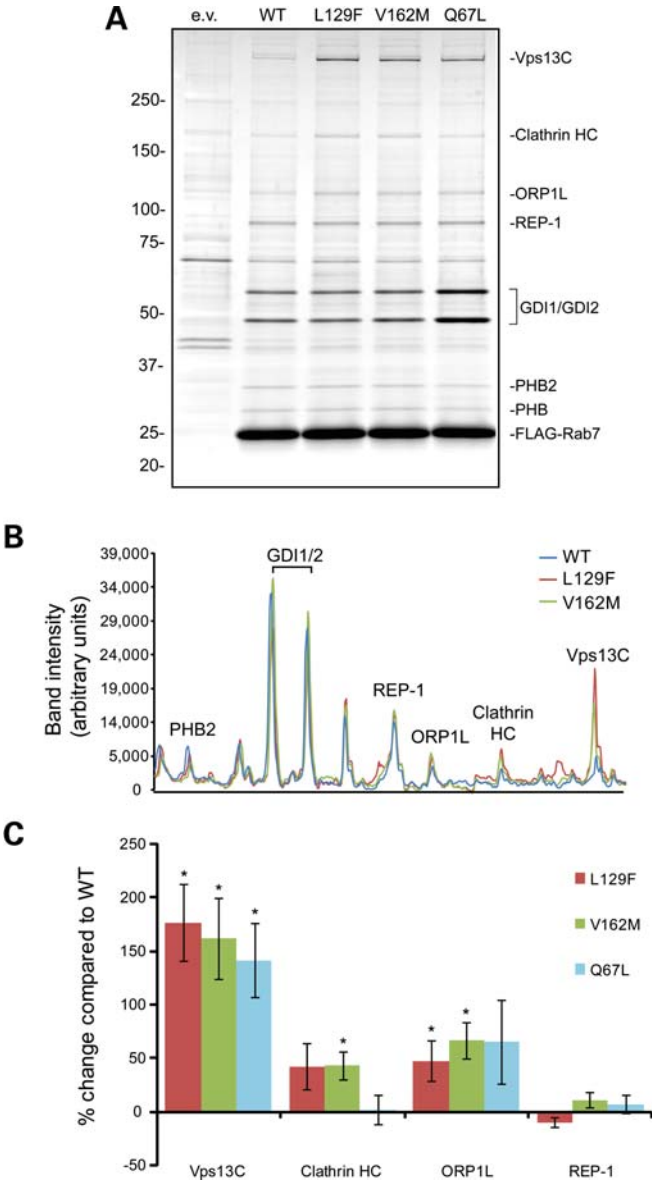

Figure 4. Rab7 disease mutants demonstrate quantitative changes in effector interactions. (**A**) FLAG–Rab7 was immunoprecipitated from HEK293T cells followed by SDS–PAGE and SYPRO Ruby protein stain. Interacting proteins were identified by LC-MS/MS. (**B**) Rab7 wild-type and disease mutants have roughly similar band intensity profiles, although a subset of protein interactors shows differential binding (compare intensity profiles for Vps13C and ORP1L). (**C**) Quantification of FLAG–Rab7 coimmunoprecipitation replicates demonstrates increased interaction of Rab7 disease mutants with Vps13C, clathrin heavy chain and ORP1L, and normal interaction with REP-1 ($^*P < 0.05$). Values plotted represent the average of five or six independent experiments. Error bars represent standard error of the mean. e.v. = empty vector.

late-endosomal/lysosomal marker LAMP2 (Fig. 5A, top) and the acidotropic dye LysoTracker Red (data not shown) as expected (6). The dominant-negative T22N mutant has a diffuse, reticular localization and leads to dispersal and altered morphology of late endosomes and lysosomes (Fig. 5A, bottom). In contrast, the constitutively active Q67L mutant Rab7 colocalizes with LAMP2, but leads to prominent

Table 2. Proteomics summary and statistics

Protein name	MW (Da)	Sequence count	Coverage (%)	Novelty
GDI2	51 088	370	76	
GDI1	51 177	255	70	
Prohibitin 2 (PHB2)	33 276	115	51	*
Prohibitin (PHB)	29 843	84	51	*
REP-1 (CHM)	74 740	77	39	
Vps13C	419 351	217	34	*
ORP1L	109 739	71	29	
VapB (ALS8)	27 365	6	25	*
Stomatin-like 2 (EPB72)	38 518	23	25	*
Clathrin HC	193 703	44	24	*
GNB2L1 (RACK1)	40 193	7	18	*
ATP6V0A1	96 487	10	13	*
Spastic paraplegia 21 (SPG21/maspardin)	35 223	7	12	*
IMMT (Mitofilin)	83 669	10	9	*
RILP	44 375	3	8	
ANKFY1	128 489	4	4	*

*Novel interactor.

accumulation of enlarged vesicles that cluster adjacent to the nucleus (Fig. 5A, middle). Surprisingly, despite evidence of unregulated activation, Rab7 disease mutants have normal subcellular localization and associate normally with LAMP2 (Fig. 5B) and LysoTracker Red (data not shown). Quantification of the cellular phenotypes verified our observation that disease mutants are similar to wild-type Rab7 and distinct from the Q67L mutant (Fig. 5C, see Supplementary Material, Fig. S6 for scoring examples). We also demonstrated that Rab7 disease mutations do not impair targeting to autophagosomes or flux through the autophagic pathway (Supplementary Material, Fig. S7). Thus, even though Rab7 disease mutants show a marked increase in the active fraction, the cellular phenotype of disease mutants is clearly distinct from the Q67L mutant (Fig. 5A–C) providing further evidence that a GTPase defect alone cannot account for the phenotype in Rab7 disease mutants.

Mutant Rab7 is abnormally retained on vesicular membranes

Rab GTPases switch between the GTP-bound state in which they are active and membrane-associated and the GDP-bound state in which they are inactive and cytosolic. Our results suggest increased activation of Rab7 disease mutants which would be predicted to correlate with alterations in the activity cycle. To assess the net impact of Rab7 mutations on membrane cycling, we used dynamic live-cell imaging to characterize wild-type and mutant GFP–Rab7 in living cells. Time-lapse images demonstrate that disease-causing mutants of Rab7 associate with vesicular structures that are highly motile and undergo multiple fusion and fission events similar to wild-type (Supplementary Material, Movies S1–S4). We next used dynamic live-cell imaging and a fluorescence recovery after photobleaching (FRAP) approach to examine how disease-causing mutations of Rab7 affect membrane cycling activity. HeLa cells were transfected with

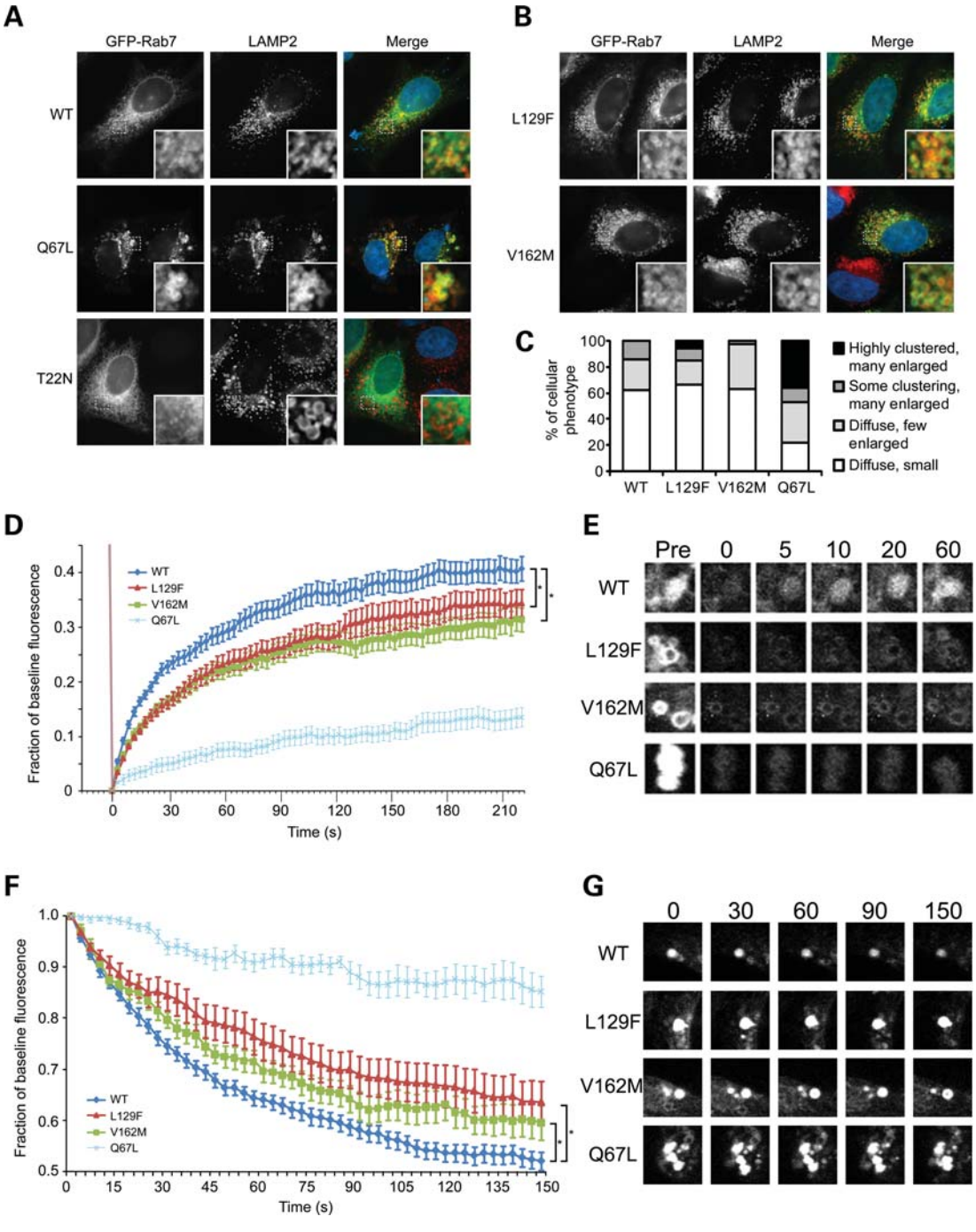

Figure 5. Rab7 disease mutants have normal subcellular localization but decreased membrane cycling. (**A**–**B**) HeLa cells transfected with GFP–Rab7 constructs were fixed and stained with anti-LAMP2 antibody. Wild-type Rab7 and disease mutants colocalize with LAMP2-positive vesicles and do not cause any alteration in their morphology or localization. In contrast, constitutively active Q67L Rab7 causes clustering of LAMP2-positive vesicles, whereas dominant-negative T22N Rab7 leads to their dispersal and enlargement. (**C**) Quantification of vesicular phenotypes in GFP–Rab7-expressing cells demonstrates that disease mutants are similar to wild-type and distinct from Q67L Rab7. Approximately 40 cells were blindly scored for each Rab7 construct (see Supplementary Material, Fig. S6 for scoring examples). (**D**) FRAP of GFP–Rab7-positive vesicles in HeLa cells demonstrates that Rab7 disease mutants have a decreased rate of fluorescence recovery compared with wild-type. As expected, constitutively active Rab7 (Q67L) shows minimal fluorescence recovery due to the inability to hydrolyze GTP. (**E**) Representative time-lapse images of GFP–Rab7 vesicles before and after photobleaching. (**F**) FLAP of photoactivatable-GFP (PA-GFP)–Rab7-positive vesicles demonstrates that Rab7 disease mutants have a decreased rate of fluorescence loss compared with wild-type. As expected, constitutively active Rab7 (Q67L) shows minimal fluorescence loss due to the inability to hydrolyze GTP. (**G**) Representative time-lapse images of PA-GFP–Rab7 vesicles after photoactivation. Values indicate average fluorescence for at least 20 ROIs in at least 10 cells for each condition ($^{*}P = 1 \times 10^{-15}$). Error bars represent standard error of the mean.

GFP–Rab7 and regions of cytosol containing GFP–Rab7-positive vesicles were bleached with a high intensity laser. As recovery of fluorescence requires that the bleached GFP–Rab7 molecules dissociate from the membrane to allow insertion of unbleached Rab7 from the surrounding cytosol, the rate of fluorescence recovery represents flux through the Rab7 activity cycle (31). Rab7 disease mutants L129F and V162M showed a small but significant decrease in the rate of fluorescence recovery compared with wild-type, whereas the constitutively active Q67L mutant showed a nearly complete loss of fluorescence recovery due to the inability to hydrolyze GTP (Fig. 5D and E). These results indicate that disease-causing mutations in Rab7 cause a subtle decrease in the rate of membrane exchange.

Decreased FRAP could result from decreased membrane extraction or from impaired recruitment of unbleached Rab7 onto target membranes. To distinguish between these possibilities, we developed a complementary approach utilizing a photoactivatable GFP variant (PA-GFP) (32) fused to Rab7. As PA-GFP fluorescence is low until activation by brief high intensity laser stimulation, this construct permits selective activation of small regions of cytosol containing Rab7-positive vesicles. In activated regions of the cell, a majority of the activated Rab7 is membrane-bound and thus the fluorescence loss after photoactivation (FLAP) specifically measures the rate of extraction of Rab7 from its target vesicle membranes. Rab7 disease mutants L129F and V162M showed a decreased rate of fluorescence loss compared with wild-type Rab7, suggesting delayed membrane extraction (Fig. 5F and G). As expected, constitutively active Rab7 (Q67L) showed a markedly decreased rate of fluorescence loss due to the inability to hydrolyze GTP. Taken together, the FRAP and FLAP data suggest that Rab7 disease-causing mutants are impaired in membrane exchange specifically due to slowed extraction from their target membranes. Notably, the decreased rate of FRAP and FLAP in disease mutants was much less pronounced than in the Q67L mutant (Fig. 5D–G). Thus, despite a profound increase in the active fraction similar to that seen in the Q67L mutant, the net impact of disease-causing mutations *in vivo* is surprisingly subtle.

GTP dissociation inactivates mutant Rab7

Our data demonstrate that despite accelerated nucleotide exchange and a marked increase in the active fraction similar to the Q67L mutant (Fig. 3), Rab7 disease mutants have normal subcellular localization and only subtle defects in membrane extraction (Fig. 5). To reconcile these observations, we hypothesized that the excessive activation in mutant Rab7 is counterbalanced by unregulated, hydrolysis-independent termination of activity mediated by accelerated GTP dissociation (Fig. 2A). To test this, we generated compound mutants containing both the Q67L mutation (which inactivates the catalytic site) and a disease-causing mutation (either L129F or V162M). We predicted that conversion from GTP-bound, active Rab7 to inactive Rab7 through GTP dissociation would rescue the function of these catalytically dead mutants. Although transfected GFP–Rab7 Q67L showed vesicular clustering in the majority of cells, the phenotype was largely reversed by introducing the disease-causing mutations to the Q67L background (Fig. 6A and B, see Supplementary Material, Fig. S6 for scoring examples). To further demonstrate reversal of the Q67L phenotype in compound mutants, we performed FRAP assays to follow the extraction of the compound mutants from membranes. We found that the Rab7 compound mutants largely rescued the FRAP defect seen in the Q67L mutant alone, suggesting that the Rab7 disease-causing mutations increase GTP dissociation and lead to GTPase-independent membrane cycling of Rab7 *in vivo* (Fig. 6C). These results further indicate that GTPase deficiency cannot account for the defects in disease mutants, because these mutations are able to reverse the phenotype associated with a pure GTPase defect. Furthermore, these data demonstrate that disease mutants are not dependent on GTP hydrolysis for inactivation as is the case for nearly all Rab GTPases. Together with our GTP exchange assays, our results indicate that Rab7 mutations lead to misregulation of both activation of Rab7 by nucleotide exchange and inactivation of Rab7 by GTP dissociation. Therefore, GTP binding and membrane cycling of Rab7 mutants occur independent of the action of the normal regulatory controls that provide spatial and temporal specificity to Rab7 function.

DISCUSSION

In this study, we characterized the structural, biochemical and cell biological consequences of mutations in the small GTPase Rab7 that cause the dominantly inherited axonal degeneration CMT2B. Examination of the crystal structure of the L129F Rab7 mutant revealed alteration of the nucleotide binding pocket but no significant alteration to the catalytic site. We demonstrated that despite rapid GTP dissociation and re-association, GTPase activity in disease mutants is not significantly reduced. We showed that disease mutations result in an increase in the active fraction of Rab7 and a corresponding increase in binding to a subset of effector proteins. In addition, we demonstrated that increased activation in disease mutants is due to unregulated nucleotide exchange and not due to a hydrolysis defect. Surprisingly, the cellular phenotype of mutant Rab7 is milder than expected given the prominent, unregulated GTP exchange and marked increase in the active fraction. To account for this, we documented that unregulated activation of Rab7 disease mutants is mitigated by unregulated inactivation. Thus, our data reveal how misregulation of multiple steps of the Rab7 activity cycle leads to the alteration of Rab7 activity. A previous publication suggested that Rab7 disease mutants lead to constitutive activation and a nearly complete loss of catalytic activity (21). However, such a severe alteration of activity would be predicted to have far-reaching effects on Rab7-dependent pathways. Indeed, overexpression of constitutively active Rab7 leads to developmental defects in *Drosophila* (33,34). Although Rab7 is ubiquitously expressed, disease mutations cause adult-onset, slowly progressive disease that is restricted to the neurons with the longest axonal projections. Our findings of subtle changes in Rab7 activity are consistent with this pattern of disease in which a slight underlying defect becomes pathological only in a subset of vulnerable neurons.

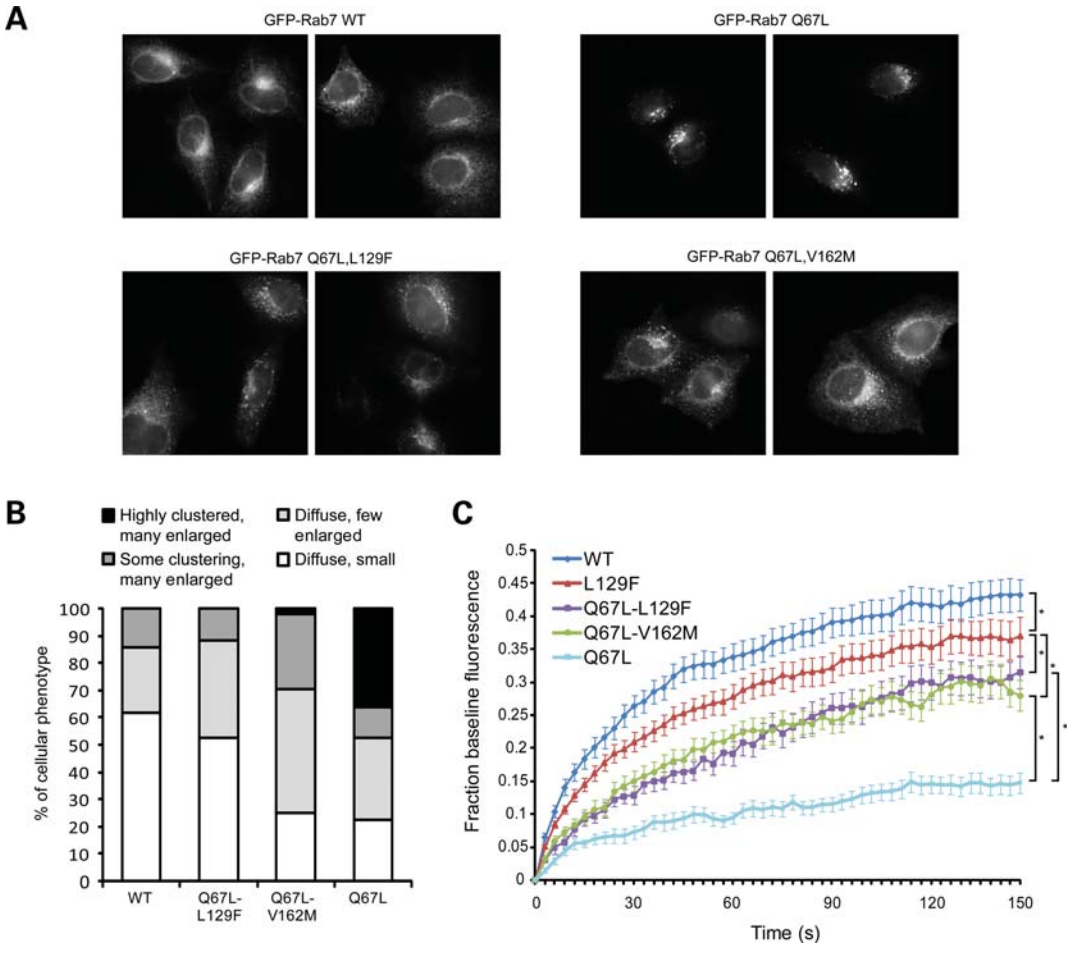

Figure 6. Rab7 disease mutants lead to GTPase-independent membrane cycling. (**A**) HeLa cells transfected with GFP–Rab7 were fixed and imaged. Rab7 Q67L,L129F or Q67L,V162M compound mutants largely rescue the abnormal vesicular clustering seen in the GTPase-deficient Q67L mutant. (**B**) Quantification of vesicular phenotypes in GFP–Rab7-expressing cells. Approximately 40 cells were blindly scored for each Rab7 construct (see Supplementary Material, Fig. S6 for scoring examples). (**C**) Compound mutants rescue the FRAP defect seen in the constitutively active Q67L mutant. Rab7 Q67L shows minimal fluorescence loss due to the inability to hydrolyze GTP. Membrane release and fluorescence recovery is restored by combining the Q67L mutation with the L129F or V162M disease mutations. Values indicate average fluorescence for at least 30 ROIs in at least 15 cells for each condition ($^{*}P < 1 \times 10^{-15}$). Error bars represent standard error of the mean.

Unregulated Rab7 cycling and accumulation of activated Rab7

Almost all Rab GTPases share two physiological properties, slow GDP dissociation and low intrinsic GTPase activity. These properties render Rabs, including Rab7, dependent on the positive and negative influences of regulatory GEF and GAP proteins. In Rab7 disease mutants, these two critical properties are absent, and Rab7 mutants are able to circumvent normal regulatory controls (Fig. 7). Specifically, we provide evidence that Rab7 mutants are able to become activated independent of GEF activity due to rapid, unregulated GTP exchange (Fig. 3), but this activation is counterbalanced by unregulated, GTPase-independent termination of activity (Fig. 6). The net effect of unregulated activation and inactivation is a subtle increase in the duration of association of active Rab7 with target membranes and an increase in the GTP-bound, active fraction (Figs. 3, 4, and 5).

Membrane cycling in mutant Rab7 is uncoupled from GTP hydrolysis

Although a previous report concluded that disease mutants have a GTPase defect (21), we demonstrate that this apparent defect is largely a reflection of increased GTP dissociation. Under conditions where GTP is provided in excess, the hydrolysis rate of disease mutants approaches that of wild-type Rab7 (Fig. 2C–E). As the physiological concentration of GTP ($\sim$500 μM) is higher than the concentrations we used in our assays (35), we predict that *in vivo*, dissociation of GTP would be followed by re-association and subsequent hydrolysis. Indeed, the observation that the phenotype of disease mutants is somewhat altered by adding the Q67L mutation (Fig. 6A–C) provides indirect evidence that a modest amount of GTP hydrolysis does occur in disease mutants *in vivo*. Otherwise, adding the GTPase mutation to the disease mutant background would have no effect on their cellular

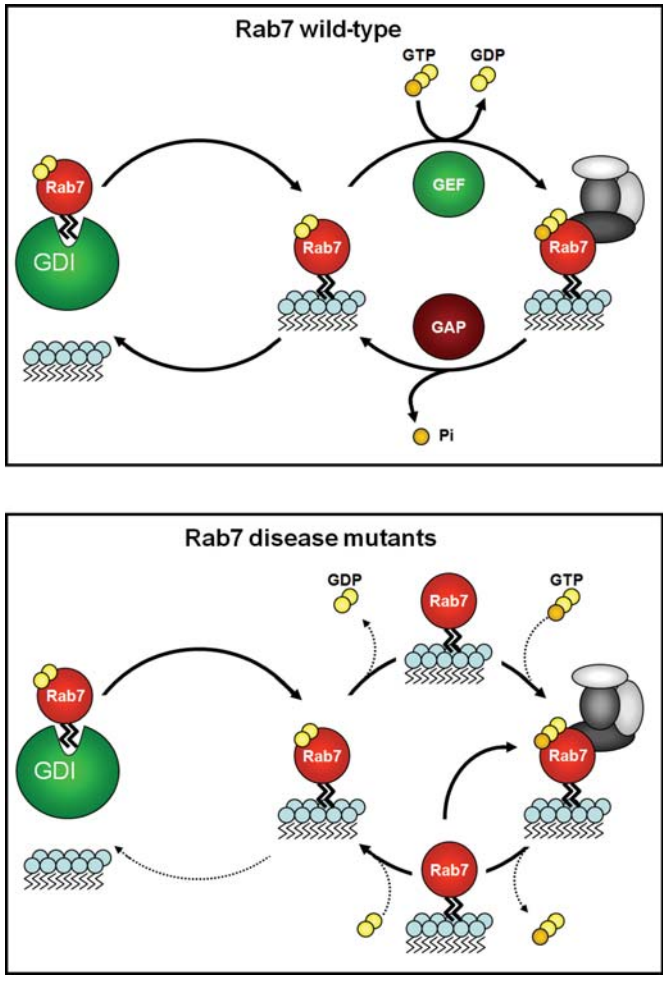

Figure 7. Model of how Rab7 disease mutants cause misregulation of the activation cycle. Activation of membrane-associated Rab7 normally requires GEF activity due to very slow dissociation of GDP. Following GTP binding, GAP-catalyzed hydrolysis inactivates Rab7 and allows extraction from the membrane by GDI. In Rab7 disease mutants, the regulation of the activity cycle is disrupted. Decreased affinity for GDP allows GTP exchange to occur independent of GEF activity, and GTP dissociation allows hydrolysis-independent inactivation of Rab7. Following GTP dissociation, Rab7 mutants can either become reactivated by binding GTP or can bind GDP and become extracted by GDI. As the relative affinity for GTP is greater than for GDP, Rab7 mutants are more likely to rebind GTP and undergo multiple activation cycles on target membranes before they are extracted. Thus, disease mutants cause misregulation of activation and inactivation of Rab7 resulting in alteration of the GTP–GDP ratio and a subtle increase in residence on target membranes. In the GTP-bound state, we predict that Rab7 disease mutants are largely bound to effectors, although it is possible that some fraction is not associated with effector proteins.

phenotype. In addition, disease mutations are also able to rescue membrane cycling in the GTPase-deficient mutant (Fig. 6C), suggesting hydrolysis-independent inactivation as a result of disease mutations. On the basis of these results, we propose that Rab7 disease mutants are able to become inactivated by two routes: (i) rapid dissociation and re-association of GTP with eventual GTP hydrolysis and (ii) dissociation of GTP and association of GDP. Both of these mechanisms of inactivation are distinct from inactivation in wild-type Rab7 and highlight how disease mutations lead to misregulation of Rab7 activity.

Rab7 mutations cause a quantitative but not qualitative change in interaction with effector proteins

Using LC-MS/MS, we demonstrate that disease-causing mutations do not qualitatively alter the complement of Rab7 interactors but cause quantitative changes in specific interactions (Fig. 4). This observation is consistent with our structural studies that reveal that the overall structure of mutant Rab7, and in particular the effector binding region, is unchanged from wild-type (Fig. 1). Specifically, we demonstrate significantly increased interaction of both Rab7 disease mutants with ORP1L, a well-characterized effector of active Rab7 that facilitates retrograde trafficking of late endosomes (36), and Vps13C, which also shows increased binding to the Q67L mutant and is likely a mediator of active Rab7 function. Vps13C is an as yet uncharacterized protein whose yeast homolog regulates trafficking to the vacuole (37). Our analysis also identified several previously unidentified potential interactors of Rab7 (Table 2). Of particular note are VapB, the FYVE containing-protein ANKFY1, and SPG21, which localize to membranes and potentially play a role in vesicular transport (38–40). A recent study elegantly demonstrated a role for VapB and VapA in regulating the cholesterol-dependent microtubule trafficking of Rab7-positive late endosomes (41). High cholesterol levels on the cytosolic face of vesicles activate ORP1L leading to stable recruitment of dynein, whereas low cholesterol levels allow the extraction of motor proteins from Rab7–RILP complexes by VapA and B. Our data suggest that misregulation of the Rab7 activity cycle in disease mutants may perturb such carefully orchestrated vesicular trafficking pathways.

Notably, two of the novel Rab7 interacting proteins we identified have been implicated in human diseases affecting the nervous system. VapB mutations cause a familial type of amyotrophic lateral sclerosis (ALS8) (42), and SPG21/maspardin mutations cause spastic paraplegia 21 (43). In addition, mutations in previously known Rab7 interactors have been implicated in multiple neurological diseases: REP-1 in choroideremia (44,45), GDI in X-linked mental retardation (46), $p150^{glued}$ in distal spinobulbar muscular atrophy (47), βIII spectrin in spinocerebellar ataxia 5 (48) and RILP as a gene deleted in Miller–Dieker syndrome (49). These results reveal a nexus of Rab7-associated proteins involved in human neurological disease and suggest that neurons are particularly vulnerable to mutations that impair protein trafficking through the endo-lysosomal system. Furthermore, the frequency with which function of the endo-lysosomal system is disrupted in familial and sporadic neurodegenerative diseases suggests overlapping mechanisms of pathogenesis, as has been suggested previously (50).

Functional consequences of Rab7 mutations

Dominantly inherited neurodegenerative diseases are typically attributed to gain-of-function mechanisms. At present, prevailing hypotheses suggest that disease results from gain of a *novel* toxic function that is unrelated to the normal function of the mutant protein. For example, many neurodegenerative diseases are caused by mutations that disrupt protein folding leading to the formation of aggregates that are potentially neurotoxic. In other cases, a dominant-negative mechanism leads

to loss-of-function of the mutant protein and its associated complexes. Our elucidation of the molecular defect caused by mutations in Rab7 illustrates an alternative mechanism: toxic misregulation of *native* function. Although there is precedent for this mechanism underlying tumorigenesis, to our knowledge, this is the first example of this type of mechanism underlying neurodegenerative disease.

How might misregulation of Rab7 lead to axonal degeneration? Rab7 specifically regulates transport, docking and fusion of late endosomes, autophagosomes and lysosomes. As such, Rab7 plays an important role in determining the fate of endocytic vesicles by regulating their fusion and subsequent degradation by lysosomes. In cultured neurons, over-expression of dominant-negative Rab7 reduces the degradation of TrkA-containing signaling endosomes leading to increased trophic signaling and excessive neurite outgrowth (9). Misregulation of Rab7 function as seen in CMT2B may have the opposite effect, resulting in premature lysosomal degradation of endocytic vesicles. CMT2B is characterized by length-dependent axonal degeneration that most prominently affects pain sensation. Notably, there is significant clinical overlap between CMT2B and familial insensitivity to pain (HSAN5, OMIM 608654) caused by loss-of-function mutations in nerve growth factor-beta (NGF-β) and also congenital insensitivity to pain with anhydrosis (OMIM 256800), which is caused by loss-of-function mutations in the NGF-β receptor TrkA (51,52). The phenotypic similarity of CMT2B to these syndromes leads us to speculate that Rab7 mutations may cause premature degradation of TrkA-containing signaling endosomes with resulting attenuation of neurotrophic support and selective axonal degeneration in a length-dependent manner. Our results provide a framework for future work examining how Rab7 mutants influence signaling endosome dynamics and vesicular trafficking in cultured neurons and animal models.

MATERIALS AND METHODS

Determination of the structure of L129F Rab7

Full-length L129F Rab7 was produced and crystallized as described in Supplementary Material. Phases were calculated by MR using PHASER (53) as implemented in CCP4 suite of programs using the substrate-free structure of Rab7 (PDB ID 1VG8) as a search model. Maps calculated after one cycle of refinement by REFMAC followed by solvent flattening and five-fold multidomain, non-crystallographic symmetry averaging using density modification (54) revealed clear *fo*−*fc* density for the nucleotide substrate at 2.5 s contour level. Model building was carried out in COOT (55), and the model was refined using both CNS-SOLVE (56) and REFMAC5 (57). The last cycles of refinement were carried out with translation, libration, screw (TLS) restraints as implemented in REFMAC5 and without NCS restraints (Table 1).

GTP/GDP dissociation assays

Wild-type, L129F, and V162M His-MBP-Rab7 fusion proteins were expressed and purified from bacteria as described in Supplementary Material, but the His-MBP tag was not cleaved. Fusion proteins were bound to NiNTA beads (Sigma-Aldrich) for 30 min at 4°C in Buffer A (20 mM Tris−HCl, 100 mM NaCl, 5 mM $MgCl_2$, 1 mM NaH_2PO_4, 10 mM 2-mercaptoethanol, pH 7.8) followed by one wash with 1 M guanidine-HCl. Bound Rab7 proteins were then incubated in Buffer A containing 0.1 μM ^{3}H-GTP or ^{3}H-GDP for 30 min on ice and washed to remove unbound nucleotide. Proteins were incubated in Buffer A containing a 1000-fold excess of unlabeled GTP or GDP for 0, 15, 30 or 60 min at 37°C. Samples were washed to remove dissociated nucleotide. To elute nucleotides, 10 μl of elution buffer (0.2% SDS, 5 mM EDTA, 5 mM GTP and 5 mM GDP) was added, and samples were incubated at 65°C for 2 min. Eluted nucleotides were quantified using scintillation counting, and the amount of ^{3}H-GTP or ^{3}H-GDP bound at 15, 30 and 60 min was compared with the initial amount bound (0 time point).

GTPase assay

His-MBP-Rab7 fusion proteins were bound to NiNTA beads as above followed by three washes with 1 M guanidine-HCl and three washes with Buffer A. Reactions were incubated with 30 μl of Buffer A containing ^{32}P-GTP for 2 h on ice to load GTP. Hydrolysis was initiated by moving the reactions to 37°C for 2 h. In some reactions, 1000-fold excess unlabeled GTP was added to the reaction during hydrolysis ('+excess unlabeled GTP' condition). Following hydrolysis, nucleotides were eluted as above. Samples were spotted on polyetherimide (PEI) cellulose and resolved in NaH_2PO_4 (pH 3.4) for ∼1 h. Signals for GTP and GDP were calculated using a PhosphorImager. The percentage of ^{32}P-GTP hydrolyzed in each experiment was calculated by dividing the GDP signal by the total signal from GTP and GDP, taking into account that the specific activity of ^{32}P-GDP is two-third that of ^{32}P-GTP.

GTP exchange assays

For the cell-free exchange assay, recombinant MBP-His-Rab7 proteins were bound, treated with guanidine-HCl, and washed as above. To determine the maximum amount of ^{3}H-GTP that could be bound, His-MBP-Rab7 proteins were incubated in Buffer A containing 0.1 μM ^{3}H-GTP for 30 min at 37°C. Following washes, bound ^{3}H-GTP was eluted and quantified as above. To determine the GTP exchange rate, His-MBP-Rab7 proteins were treated as above except incubated in Buffer A containing 0.2 mM unlabeled GDP before the addition of ^{3}H-GTP. Following washes, Buffer A containing ^{3}H-GTP was added, and the proteins were incubated at 37°C for 10 or 30 min. Samples were washed and eluted nucleotide was quantified as above. The ratio of the amount of ^{3}H-GTP bound at 10 or 30 min to the maximum amount bound without GDP pre-incubation was calculated for wild-type, L129F and V162M Rab7. For the exchange assay from cell lysates, HEK293T cells were transfected with FLAG−Rab7, and cells were harvested 48 h post-transfection and lysed in IP buffer [20 mM HEPES, 10% glycerol, 0.5% Triton X-100, 150 mM NaCl, 2 mM $MgCl_2$, 1 mM DTT and Complete Mini Protease Inhibitor Cocktail EDTA-free (Roche)]. Rab7 proteins were immunopurified using FLAG-M2 agarose

(Sigma-Aldrich) and washed several times in IP buffer. Immunopurified Rab7 proteins were then incubated in IP buffer containing 0.1 μM ^{3}H-GTP for 10 min at 37°C. Following several washes, bound nucleotides were eluted and quantified as above.

LC-MS/MS protein identification

HEK293T cells were transfected with FLAG–Rab7 constructs and immunoprecipitated as above, and proteins were separated by SDS–PAGE and stained with SYPRO Ruby (Sigma-Aldrich). Bands were then excised, digested, processed and analyzed as described in Supplementary Material.

FRAP

For Figure 5, HeLa cells were plated in 35 mm cover slip-bottom dishes (MatTek) and transfected with GFP–Rab7 constructs. Live-cell imaging was performed 24 h post-transfection using a FluoView FV1000 Olympus laser scanning confocal microscope under 60× oil immersion. Cells were imaged every 3 s for 15 s total using the Argon ion 488 nm laser (30 mW) at 1% excitation power to record the pre-bleach fluorescence levels. Small regions of the cytosol containing GFP–Rab7 vesicles were then bleached using the 488 nm laser at 100% power for 2 s. Recovery of fluorescence was monitored every 3 s for 225 s using the 488 nm laser at 1% power. Regions of interest (ROIs) were drawn around bleached Rab7 vesicles and the fluorescence intensity at each time point was calculated using Metamorph software. Fluorescence intensity values were exported to Microsoft Excel and fluorescence recovery curves from each condition were averaged and plotted. Pre-bleach fluorescence was set to 1 and the first post-bleach time point was set to 0 for each ROI. For FRAP of compound mutants (Fig. 6), cells were plated and transfected as above, and imaged using a Nikon TE2000 microscope with a C1Si confocal using the 60× oil immersion objective. Pre- and post-bleach excitation was performed with a 488 nm diode laser at 2% power every 3 s for 5 and 50 frames, respectively. Photobleaching was performed at 100% laser power for 10 s. Data were analyzed using EZC1 software, then exported to Microsoft Excel and graphed as above.

FLAP

HeLa cells were plated as in FRAP assays and transfected with PA-GFP–Rab7 constructs. Live-cell imaging was performed 24 h post-transfection using a FluoView FV1000 Olympus laser scanning confocal microscope. Regions of cytosol containing PA-GFP–Rab7 vesicles were identified using the 488 nm laser at 10% power. Small regions were then activated by a 2 s pulse with the violet diode 405 nm laser (25 mW) at 50% power. Loss of fluorescence was monitored every 3 s for 150 s using the 488 nm laser at 1% power (at this power, unactivated PA-GFP fluorescence is undetectable). ROIs were drawn around activated Rab7 vesicles and the fluorescence intensity was plotted over time as in FRAP assays. The first post-bleach time point was set to 1 for each ROI. Fluorescence loss curves from each condition were averaged and plotted. See Supplementary Material, for additional methods.

SUPPLEMENTARY MATERIAL

Supplementary Material is available at *HMG* online.

ACKNOWLEDGEMENTS

We thank Andrew Gillis and Meghan Mitchell for help in generating purified Rab7 for crystallization, Chunxu Qu for help in statistical analysis, Jennifer Peters, Samuel Connell, and Haji Takano for help with FRAP experiments, and Natalia Nedelsky and Brett Winborn for helpful comments and critical review of the manuscript. We thank Vincent Timmerman, Jacques Neefjes, Zakaria Hmama, Jennifer Lippincott-Schwartz, Aimee Edinger and Cecilia Bucci for providing critical reagents. We thank the Hartwell Center Proteomics Core for protein identification by LC-MS/MS and the Hartwell Center Protein Production Core for generating recombinant Rab7 proteins. Author contributions: B.A.M. and J.P.T conceived of and designed the study. B.A.M. conducted the study. E.S. contributed to collection and interpretation of structural data. B.A.M. and J.P.T. wrote the manuscript with contributions from E.S.

Conflict of Interest statement. None declared.

FUNDING

Financial support was provided by training grant T32AG000255, the Dana Foundation and ALSAC (American Lebanese Syrian Associated Charities). Funding to pay the Open Access publication charges for this article was provided by ALSAC.

REFERENCES

1. Sasaki, T., Kikuchi, A., Araki, S., Hata, Y., Isomura, M., Kuroda, S. and Takai, Y. (1990) Purification and characterization from bovine brain cytosol of a protein that inhibits the dissociation of GDP from and the subsequent binding of GTP to smg p25A, a ras p21-like GTP-binding protein. *J. Biol. Chem.*, **265**, 2333–2337.
2. Rak, A., Pylypenko, O., Durek, T., Watzke, A., Kushnir, S., Brunsveld, L., Waldmann, H., Goody, R.S. and Alexandrov, K. (2003) Structure of Rab GDP-dissociation inhibitor in complex with prenylated YPT1 GTPase. *Science*, **302**, 646–650.
3. Sato, Y., Fukai, S., Ishitani, R. and Nureki, O. (2007) Crystal structure of the Sec4p.Sec2p complex in the nucleotide exchanging intermediate state. *Proc. Natl Acad. Sci. USA*, **104**, 8305–8310.
4. Ullrich, O., Stenmark, H., Alexandrov, K., Huber, L.A., Kaibuchi, K., Sasaki, T., Takai, Y. and Zerial, M. (1993) Rab GDP dissociation inhibitor as a general regulator for the membrane association of rab proteins. *J. Biol. Chem.*, **268**, 18143–18150.
5. Feng, Y., Press, B. and Wandinger-Ness, A. (1995) Rab 7: an important regulator of late endocytic membrane traffic. *J. Cell Biol.*, **131**, 1435–1452.
6. Bucci, C., Thomsen, P., Nicoziani, P., McCarthy, J. and van Deurs, B. (2000) Rab7: a key to lysosome biogenesis. *Mol. Biol. Cell*, **11**, 467–480.
7. Harrison, R.E., Bucci, C., Vieira, O.V., Schroer, T.A. and Grinstein, S. (2003) Phagosomes fuse with late endosomes and/or lysosomes by extension of membrane protrusions along microtubules: role of Rab7 and RILP. *Mol. Cell. Biol.*, **23**, 6494–6506.

8. Vitelli, R., Santillo, M., Lattero, D., Chiariello, M., Bifulco, M., Bruni, C.B. and Bucci, C. (1997) Role of the small GTPase Rab7 in the late endocytic pathway. *J. Biol. Chem.*, **272**, 4391–4397.
9. Saxena, S., Bucci, C., Weis, J. and Kruttgen, A. (2005) The small GTPase Rab7 controls the endosomal trafficking and neuritogenic signaling of the nerve growth factor receptor TrkA. *J. Neurosci.*, **25**, 10930–10940.
10. Ceresa, B.P. and Bahr, S.J. (2006) rab7 activity affects epidermal growth factor:epidermal growth factor receptor degradation by regulating endocytic trafficking from the late endosome. *J. Biol. Chem.*, **281**, 1099–1106.
11. Gutierrez, M.G., Munafo, D.B., Beron, W. and Colombo, M.I. (2004) Rab7 is required for the normal progression of the autophagic pathway in mammalian cells. *J. Cell Sci.*, **117**, 2687–2697.
12. Jager, S., Bucci, C., Tanida, I., Ueno, T., Kominami, E., Saftig, P. and Eskelinen, E.L. (2004) Role for Rab7 in maturation of late autophagic vacuoles. *J. Cell Sci.*, **117**, 4837–4848.
13. Deinhardt, K., Salinas, S., Verastegui, C., Watson, R., Worth, D., Hanrahan, S., Bucci, C. and Schiavo, G. (2006) Rab5 and Rab7 control endocytic sorting along the axonal retrograde transport pathway. *Neuron*, **52**, 293–305.
14. Zweifel, L.S., Kuruvilla, R. and Ginty, D.D. (2005) Functions and mechanisms of retrograde neurotrophin signalling. *Nat. Rev. Neurosci.*, **6**, 615–625.
15. Barisic, N., Claeys, K.G., Sirotkovic-Skerlev, M., Lofgren, A., Nelis, E., De Jonghe, P. and Timmerman, V. (2008) Charcot-Marie-Tooth disease: a clinico-genetic confrontation. *Ann. Hum. Genet.*, **72**, 416–441.
16. Zuchner, S. and Vance, J.M. (2006) Mechanisms of disease: a molecular genetic update on hereditary axonal neuropathies. *Nat. Clin. Pract. Neurol.*, **2**, 45–53.
17. Houlden, H., King, R.H., Muddle, J.R., Warner, T.T., Reilly, M.M., Orrell, R.W. and Ginsberg, L. (2004) A novel RAB7 mutation associated with ulcero-mutilating neuropathy. *Ann. Neurol.*, **56**, 586–590.
18. Verhoeven, K., De Jonghe, P., Coen, K., Verpoorten, N., Auer-Grumbach, M., Kwon, J.M., FitzPatrick, D., Schmedding, E., De Vriendt, E., Jacobs, A. *et al.* (2003) Mutations in the small GTP-ase late endosomal protein RAB7 cause Charcot-Marie-Tooth type 2B neuropathy. *Am. J. Hum. Genet.*, **72**, 722–727.
19. Meggouh, F., Bienfait, H.M., Weterman, M.A., de Visser, M. and Baas, F. (2006) Charcot-Marie-Tooth disease due to a de novo mutation of the *RAB7* gene. *Neurology*, **67**, 1476–1478.
20. Auer-Grumbach, M., De Jonghe, P., Wagner, K., Verhoeven, K., Hartung, H.P. and Timmerman, V. (2000) Phenotype–genotype correlations in a CMT2B family with refined 3q13–q22 locus. *Neurology*, **55**, 1552–1557.
21. Spinosa, M.R., Progida, C., De Luca, A., Colucci, A.M., Alifano, P. and Bucci, C. (2008) Functional characterization of Rab7 mutant proteins associated with Charcot-Marie-Tooth type 2B disease. *J. Neurosci.*, **28**, 1640–1648.
22. Rak, A., Pylypenko, O., Niculae, A., Pyatkov, K., Goody, R.S. and Alexandrov, K. (2004) Structure of the Rab7:REP-1 complex: insights into the mechanism of Rab prenylation and choroideremia disease. *Cell*, **117**, 749–760.
23. Romero Rosales, K., Peralta, E.R., Guenther, G.G., Wong, S.Y. and Edinger, A.L. (2009) Rab7 activation by growth factor withdrawal contributes to the induction of apoptosis. *Mol. Biol. Cell*, **20**, 2831–2840.
24. Regazzi, R., Kikuchi, A., Takai, Y. and Wollheim, C.B. (1992) The small GTP-binding proteins in the cytosol of insulin-secreting cells are complexed to GDP dissociation inhibitor proteins. *J. Biol. Chem.*, **267**, 17512–17519.
25. Andres, D.A., Seabra, M.C., Brown, M.S., Armstrong, S.A., Smeland, T.E., Cremers, F.P. and Goldstein, J.L. (1993) cDNA cloning of component A of Rab geranylgeranyl transferase and demonstration of its role as a Rab escort protein. *Cell*, **73**, 1091–1099.
26. Cantalupo, G., Alifano, P., Roberti, V., Bruni, C.B. and Bucci, C. (2001) Rab-interacting lysosomal protein (RILP): the Rab7 effector required for transport to lysosomes. *EMBO J.*, **20**, 683–693.
27. Mizuno, K., Kitamura, A. and Sasaki, T. (2003) Rabring7, a novel Rab7 target protein with a RING finger motif. *Mol. Biol. Cell*, **14**, 3741–3752.
28. Stein, M.P., Feng, Y., Cooper, K.L., Welford, A.M. and Wandinger-Ness, A. (2003) Human VPS34 and p150 are Rab7 interacting partners. *Traffic*, **4**, 754–771.
29. Johansson, M., Lehto, M., Tanhuanpaa, K., Cover, T.L. and Olkkonen, V.M. (2005) The oxysterol-binding protein homologue ORP1L interacts with Rab7 and alters functional properties of late endocytic compartments. *Mol. Biol. Cell*, **16**, 5480–5492.
30. Rojas, R., van Vlijmen, T., Mardones, G.A., Prabhu, Y., Rojas, A.L., Mohammed, S., Heck, A.J., Raposo, G., van der Sluijs, P. and Bonifacino, J.S. (2008) Regulation of retromer recruitment to endosomes by sequential action of Rab5 and Rab7. *J. Cell Biol.*, **183**, 513–526.
31. Jordens, I., Fernandez-Borja, M., Marsman, M., Dusseljee, S., Janssen, L., Calafat, J., Janssen, H., Wubbolts, R. and Neefjes, J. (2001) The Rab7 effector protein RILP controls lysosomal transport by inducing the recruitment of dynein–dynactin motors. *Curr. Biol.*, **11**, 1680–1685.
32. Patterson, G.H. and Lippincott-Schwartz, J. (2002) A photoactivatable GFP for selective photolabeling of proteins and cells. *Science*, **297**, 1873–1877.
33. Wilkin, M., Tongngok, P., Gensch, N., Clemence, S., Motoki, M., Yamada, K., Hori, K., Taniguchi-Kanai, M., Franklin, E., Matsuno, K. *et al.* (2008) *Drosophila* HOPS and AP-3 complex genes are required for a Deltex-regulated activation of notch in the endosomal trafficking pathway. *Dev, Cell*, **15**, 762–772.
34. Entchev, E.V., Schwabedissen, A. and Gonzalez-Gaitan, M. (2000) Gradient formation of the TGF-beta homolog Dpp. *Cell*, **103**, 981–991.
35. Traut, T.W. (1994) Physiological concentrations of purines and pyrimidines. *Mol. Cell. Biochem.*, **140**, 1–22.
36. Johansson, M., Rocha, N., Zwart, W., Jordens, I., Janssen, L., Kuijl, C., Olkkonen, V.M. and Neefjes, J. (2007) Activation of endosomal dynein motors by stepwise assembly of Rab7–RILP-p150Glued, ORP1L, and the receptor betalll spectrin. *J. Cell Biol.*, **176**, 459–471.
37. Brickner, J.H. and Fuller, R.S. (1997) SOI1 encodes a novel, conserved protein that promotes TGN-endosomal cycling of Kex2p and other membrane proteins by modulating the function of two TGN localization signals. *J. Cell Biol.*, **139**, 23–36.
38. Kuriyama, H., Asakawa, S., Minoshima, S., Maruyama, H., Ishii, N., Ito, K., Gejyo, F., Arakawa, M., Shimizu, N. and Kuwano, R. (2000) Characterization and chromosomal mapping of a novel human gene, ANKHZN. *Gene*, **253**, 151–160.
39. Hanna, M.C. and Blackstone, C. (2009) Interaction of the SPG21 protein ACP33/maspardin with the aldehyde dehydrogenase ALDH16A1. *Neurogenetics*, **10**, 217–228.
40. Soussan, L., Burakov, D., Daniels, M.P., Toister-Achituv, M., Porat, A., Yarden, Y. and Elazar, Z. (1999) ERG30, a VAP-33-related protein, functions in protein transport mediated by COPI vesicles. *J. Cell Biol.*, **146**, 301–311.
41. Rocha, N., Kuijl, C., van der Kant, R., Janssen, L., Houben, D., Janssen, H., Zwart, W. and Neefjes, J. (2009) Cholesterol sensor ORP1L contacts the ER protein VAP to control Rab7–RILP-p150 Glued and late endosome positioning. *J. Cell Biol.*, **185**, 1209–1225.
42. Nishimura, A.L., Mitne-Neto, M., Silva, H.C., Richieri-Costa, A., Middleton, S., Cascio, D., Kok, F., Oliveira, J.R., Gillingwater, T., Webb, J. *et al.* (2004) A mutation in the vesicle-trafficking protein VAPB causes late-onset spinal muscular atrophy and amyotrophic lateral sclerosis. *Am. J. Hum. Genet.*, **75**, 822–831.
43. Simpson, M.A., Cross, H., Proukakis, C., Pryde, A., Hershberger, R., Chatonnet, A., Patton, M.A. and Crosby, A.H. (2003) Maspardin is mutated in mast syndrome, a complicated form of hereditary spastic paraplegia associated with dementia. *Am. J. Hum. Genet.*, **73**, 1147–1156.
44. van den Hurk, J.A., van de Pol, T.J., Molloy, C.M., Brunsmann, F., Ruther, K., Zrenner, E., Pinckers, A.J., Pawlowitzki, I.H., Bleeker-Wagemakers, E.M., Wieringa, B. *et al.* (1992) Detection and characterization of point mutations in the choroideremia candidate gene by PCR-SSCP analysis and direct DNA sequencing. *Am. J. Hum. Genet.*, **50**, 1195–1202.
45. Seabra, M.C., Brown, M.S. and Goldstein, J.L. (1993) Retinal degeneration in choroideremia: deficiency of rab geranylgeranyl transferase. *Science*, **259**, 377–381.
46. D'Adamo, P., Menegon, A., Lo Nigro, C., Grasso, M., Gulisano, M., Tamanini, F., Bienvenu, T., Gedeon, A.K., Oostra, B., Wu, S.K. *et al.* (1998) Mutations in GDI1 are responsible for X-linked non-specific mental retardation. *Nat. Genet.*, **19**, 134–139.
47. Puls, I., Jonnakuty, C., LaMonte, B.H., Holzbaur, E.L., Tokito, M., Mann, E., Floeter, M.K., Bidus, K., Drayna, D., Oh, S.J. *et al.* (2003) Mutant dynactin in motor neuron disease. *Nat. Genet.*, **33**, 455–456.
48. Ikeda, Y., Dick, K.A., Weatherspoon, M.R., Gincel, D., Armbrust, K.R., Dalton, J.C., Stevanin, G., Durr, A., Zuhlke, C., Burk, K. *et al.* (2006)

Spectrin mutations cause spinocerebellar ataxia type 5. *Nat. Genet.*, **38**, 184–190.
49. Cardoso, C., Leventer, R.J., Ward, H.L., Toyo-Oka, K., Chung, J., Gross, A., Martin, C.L., Allanson, J., Pilz, D.T., Olney, A.H. *et al.* (2003) Refinement of a 400-kb critical region allows genotypic differentiation between isolated lissencephaly, Miller–Dieker syndrome, and other phenotypes secondary to deletions of 17p13.3. *Am. J. Hum. Genet.*, **72**, 918–930.
50. Nixon, R.A., Yang, D.S. and Lee, J.H. (2008) Neurodegenerative lysosomal disorders: a continuum from development to late age. *Autophagy*, **4**, 590–599.
51. Einarsdottir, E., Carlsson, A., Minde, J., Toolanen, G., Svensson, O., Solders, G., Holmgren, G., Holmberg, D. and Holmberg, M. (2004) A mutation in the nerve growth factor beta gene (NGFB) causes loss of pain perception. *Hum. Mol. Genet.*, **13**, 799–805.
52. Indo, Y., Tsuruta, M., Hayashida, Y., Karim, M.A., Ohta, K., Kawano, T., Mitsubuchi, H., Tonoki, H., Awaya, Y. and Matsuda, I. (1996) Mutations in the TRKA/NGF receptor gene in patients with congenital insensitivity to pain with anhidrosis. *Nat. Genet.*, **13**, 485–488.
53. Potterton, E., Briggs, P., Turkenburg, M. and Dodson, E. (2003) A graphical user interface to the CCP4 program suite. *Acta Crystallogr. D. Biol. Crystallogr.*, **59**, 1131–1137.
54. Cowtan, K. (1994) A CCP4 density modification package. *Joint CCP4 and ESF-EACBM Newsletter on Protein Crystallography*, **31**, 34–38.
55. Emsley, P. and Cowtan, K. (2004) Coot: model-building tools for molecular graphics. *Acta Crystallogr. D. Biol. Crystallogr.*, **60**, 2126–2132.
56. Brunger, A.T., Adams, P.D., Clore, G.M., DeLano, W.L., Gros, P., Grosse-Kunstleve, R.W., Jiang, J.S., Kuszewski, J., Nilges, M., Pannu, N.S. *et al.* (1998) Crystallography & NMR system: a new software suite for macromolecular structure determination. *Acta Crystallogr. D. Biol. Crystallogr.*, **54**, 905–921.
57. Murshudov, G.N., Vagin, A.A. and Dodson, E.J. (1997) Refinement of macromolecular structures by the maximum-likelihood method. *Acta Crystallogr. D. Biol. Crystallogr.*, **53**, 240–255.